Stem Cells Translational Medicine, 2022, **11**, 1151–1164
https://doi.org/10.1093/stcltm/szac069
Advance access publication 29 September 2022
Original Research

Autophagy Enhances Longevity of Induced Pluripotent Stem Cell-Derived Endothelium via mTOR-Independent ULK1 Kinase

Katherine E. Hekman[1,2,3], Kyle M. Koss [4,5], David Z. Ivancic[5], Congcong He[6], Jason A. Wertheim[*,4,5,7]

[1]Division of Vascular Surgery and Endovascular Therapy, Department of Surgery, Emory School of Medicine, Emory University, Atlanta, GA, USA
[2]Division of Vascular Surgery, Department of Surgery, Feinberg School of Medicine, Northwestern University, Chicago, IL, USA
[3]Section of Vascular Surgery, Surgery Service Line, Atlanta VA Healthcare System, Decatur, GA, USA
[4]Department of Surgery, University of Arizona College of Medicine, Tucson, AZ, USA
[5]Comprehensive Transplant Center, Feinberg School of Medicine, Northwestern University, Chicago, IL, USA
[6]Department of Cell and Developmental Biology, Feinberg School of Medicine, Northwestern University, Chicago, IL, USA
[7]Surgery Service Line, Southern Arizona VA Healthcare System, Tucson, AZ, USA

*Corresponding author: Jason A. Wertheim, MD PhD, FACS; University of Arizona College of Medicine, 1501 N. Campbell Ave., P.O. Box 245017, Tucson, AZ 85724, USA. Tel: +1 520 626 5675; Fax: +1 520 626 6252; Email: jwertheim@arizona.edu

Abstract

Stem cells are enabling an improved understanding of the peripheral arterial disease, and patient-specific stem cell-derived endothelial cells (ECs) present major advantages as a therapeutic modality. However, applications of patient-specific induced pluripotent stem cell (iPSC)-derived ECs are limited by rapid loss of mature cellular function in culture. We hypothesized that changes in autophagy impact the phenotype and cellular proliferation of iPSC-ECs. Endothelial cells were differentiated from distinct induced pluripotent stem cell lines in 2D culture and purified for CD144 positive cells. Autophagy, mitochondrial morphology, and proliferation were characterized during differentiation and over serial passages in culture. We found that autophagy activity was stimulated during differentiation but stagnated in mature iPSC-ECs. Mitochondria remodeled through mitophagy during differentiation and demonstrated increasing membrane potential and mass through serial passages; however, these plateaued, coinciding with decreased proliferation. To evaluate for oxidative damage, iPSC-ECs were alternatively grown under hypoxic culture conditions; however, hypoxia only transiently improved the proliferation. Stimulating mTOR-independent ULK1-mediated autophagy with a plant derivative AMP kinase activator Rg2 significantly improved proliferative capacity of iPSC-ECs over multiple passages. Therefore, autophagy, a known mediator of longevity, played an active role in remodeling mitochondria during maturation from pluripotency to a terminally differentiated state. Autophagy failed to compensate for increasing mitochondrial mass over serial passages, which correlated with loss of proliferation in iPSC-ECs. Stimulating ULK1-kinase-driven autophagy conferred improved proliferation and longevity over multiple passages in culture. This represents a novel approach to overcoming a major barrier limiting the use of iPSC-ECs for clinical and research applications.

Key words: endothelial cell; mitochondria; rapamycin; senescence; tissue engineering; vascular tissue.

Received: 13 October 2021; Accepted: 23 July 2022.

Graphical Abstract

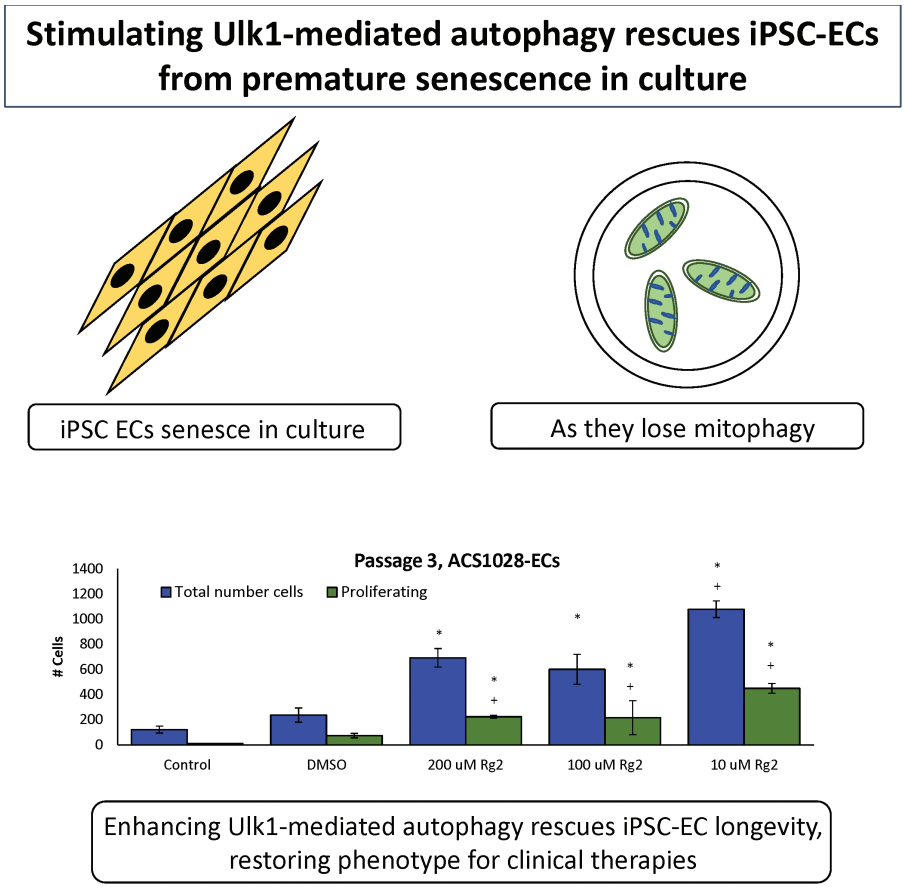

Significance Statement

This study addresses a major functional barrier to utilizing patient-specific induced pluripotent stem cell-derived endothelial cells for organ engineering and other clinical applications. These stem cell-derived vascular cells lose their mature phenotype rapidly in culture due to a loss of mitophagy and accumulation of mitochondria. This can be overcome by increasing autophagy activity, rendering them stable and longer lived for implementation in clinical applications. This removes a blockade in vascularizing more complex organs and in generating more advanced personalized therapies for vascular disease.

Introduction

Derivation of patient-specific endothelial cells and vascular tissue from induced pluripotent stem cells (iPSCs) represents a powerful tool for the study, diagnosis, and treatment of peripheral arterial disease. At present this tool remains limited by the loss of mature cellular phenotypes and degenerative changes within the cellular progeny derived from iPSCs, ultimately culminating in senescence.[1,2] Modulation of this senescence may lead to improved functionality and a more robust and durable phenotype of the resulting terminally differentiated progeny.

Endothelial cells differentiated from human iPSCs and from human embryonic stem cells via embryoid bodies typically do not retain mature endothelial cell surface markers for more than 2 weeks.[3] More recently, generating iPSC-ECs as 3-dimensional organoids appear to improve the longevity of the resulting cells; however, the applicability of this method to complex tissue and organ engineering remains to be demonstrated.[4] Multiple stimulators of autophagy activity, such as lentiviral-mediated overexpression of the longevity gene *sirtuin1* (SIRT1) as well as nutrient starvation, each attenuate premature senescence in iPSC-derived endothelial cells (iPSC-ECs) in conventional approaches to EC differentiation.[5,6] However, the precise mechanisms by which these interventions attenuate premature senescence are poorly understood.

In this study, we aim to identify the impact of autophagy, that is, the process of cellular self-digestion that recycles intracellular components, during the differentiation and culture of iPSC-ECs. During the course of unraveling the role of autophagy in iPSC-ECs, our findings uncovered alternative targets for overcoming this premature proliferative senescence. Longer-lived iPSC-ECs with a more robust functional phenotype will be imperative to advance their utility as a diagnostic and therapeutic tool in the study and treatment of human disease.

Materials and Methods

Cell Lines and Stem Cell Culture

The iPSC line ACS1028 was obtained from ATCC (ATCC-BXS0114) and were cultured on vitronectin-coated plates (Thermo Fisher A31804) with E8 flex media (Gibco

A2858501). The iPSC line Y6 was provided by the Yale University Stem Cell Center, and the cells were cultured on Matrigel-coated plates (Fisher Scientific 08-774-552) with MtESR1 media (Stem Cell Technologies 85850). Passages 10–25 were used in all experiments. Cells were passaged with ReLESR (Stem Cell Technologies 05872) and plated with 10 μM rock inhibitor (R&D 1254) for 24 h. Both lines were sent to IDEXX for STR validation, but neither existed in the repository. Routine cytogenetics and mycoplasma testing (Lonza LT07-318) were performed.

Endothelial Cell Differentiation and Maintenance

Directed differentiation of pluripotent stem cells to endothelial cells was performed according to the published protocol by the Cowan lab, using CHIR09921 (R&D 4423), BMP4 (Peprotech 120-05), forskolin (Abcam ab120058), and VEGF165 (Peprotech 100-20).[7] Endothelial cells were maintained in Vasculife VEGF media (Lifeline Cell Technology LL-0003). CD144 positive cells were separated by magnetic associated cell sorting (MACS) using CD144-conjugated magnetic beads (Miltenyi 130-097-857) in LS columns (Miltenyi 130-042-401). Purified iPSC-ECs were plated on fibronectin (Fisher Scientific CB-40008A) coated plates. iPSC-ECs were passaged with 0.025% trypsin and trypsin neutralizing solution (Lonza CC-5012 and CC-5002, respectively).

Immunostaining

Immunostaining was performed by fixing cells in 4% paraformaldehyde for 15 min at room temperature and then washing with PBS. Cells were then permeabilized with 70% ice-cold ethanol on ice and blocked with 0.5% BSA in PBS for 15 min at room temperature. Cells were then incubated overnight at 4 °C with the primary antibody in antibody dilution buffer (0.05% BSA in PBS) at the following concentrations: Nanog (Life Technologies PA1-097, 1:100), SSEA4 (Life Technologies 414000, 1:400), Sox2 (Life Technologies PA1-16968, 1:100), VE-cadherin/CD144 (Sigma V1514, 1:200), PECAM1/CD31 (Abcam ab187377, 1:100). The isotype control antibodies used in this study were mouse IgG1 (Abcam ab172730) and rabbit serum. Cells were washed with PBS and incubated with conjugated secondary antibodies at room temperature in the dark (Life Technologies, 1:300).

Flow Cytometry

Cells were lifted with Accutase (Stem Cell Technologies 07922) and stained with blue fixable live/dead stain (Invitrogen L34961 or L23105). Cells were then fixed with 4% PFA for 15 min at room temperature. For Nanog (BD Biosciences 560483) and Oct4 (Novus Biologicals NB100-2379) staining, cells were permeabilized with 0.1% Triton X-100 for 15 min on ice and blocked with 1% BSA/PBS on ice for 30 min. Cells were then incubated with the conjugated primary antibodies, 20 μL of antibody for 1×10^6 cells in 100 μL of 1% BSA/PBS. For CD144 and CD31 (BD Biosciences 560410 and 560984, respectively), fixed cells were incubated with the conjugated primary antibody, 20 μL of antibody for 1×10^6 cells in 100 μL of 1% BSA/PBS. Cells were then washed 3 times with 1% BSA/PBS. Flow cytometry was performed on the BD LSR Fortessa and analyzed in FloJo v10.

Cell Proliferation Assay

Proliferating cells were labeled with EdU using the Invitrogen Click-iT microplate assay kit (Invitrogen C10214), without the use of the Amplex Ultra red step. Cells were labeled for 24 h with 10 μM EdU or DMSO as a vehicle control. Cells were fixed and prepared according to the manufacturer's instructions, minus the Amplex Ultra red labeling. Hoechst 33342 was added at 5 μg/mL (Invitrogen H1399), and labeled cells were imaged on a Zeiss inverted fluorescence microscope. Four tiled images at 10× magnification were collected each well of 3 biological replicates per condition and stitched together as a single image per well for analysis. EdU-labeled and total nuclei were counted in Fiji.

Western Blotting

Western blotting was performed using a modified Novus Biological protocol (NB100-2220) with 10%, 12%, 14%, or 4%–20% gradient SDS-PAGE gels. Briefly, cells were collected and lysed with RIPA buffer plus PMSF protease inhibitor. The cell lysate was centrifuged at high speed for 10 min at 4 °C, and the supernatant was transferred to a fresh tube. The total protein content was quantified with a Bradford assay, and a total of 20 μg of protein was mixed with Laemmli buffer (4% SDS, 5% 2-mercaptoethanol (BME), 20% glycerol, 0.004% bromophenol blue, 0.125 M Tris HCl, pH 6.8) and denatured for 10 min at 95 °C. This was followed by wet transfer to PVDF immobilon membrane (Millipore IPFL00010) and blocked with Odyssey TBS blocking buffer (LiCor 927-50000). The following primary antibodies were used in the listed concentrations: LC3 (Novus Biologicals NB100-2220, 1:500) and GAPDH (Sigma–Aldrich G9545, 1:10 000). The LiCor IR secondaries were used 1:10 000 or 1:20 000 (LiCor 926-32211, 926-68071, and 926-32210). Bands were quantified and normalized by a ratio of LC3-II:GAPDH, rather than LC3-II:LC3-I as LC3-II is more sensitive in blotting and accurate observed alone.[8]

MitoTracker Staining

MitoTracker red (Thermo Fisher M22425) and green (Thermo Fisher M7514) were purchased from Thermo Fisher. MitoTracker red was diluted to 500 nM and MitoTracker green to 200 nM in Vasculife VEGF, along with Hoechst 33342 at 5 μg/mL (Invitrogen H1399). Live cells were incubated with the diluted dyes for 30 min at 37 °C in the dark in a humidified 5% CO_2 incubator. Cells were then washed with 1× PBS and fresh media was replaced. Cells were then imaged at 20× on a Zeiss inverted fluorescence microscope, 5 high power fields for each of 3 biological replicates, as well as an unstained control.

Transmission Electron Microscopy

Therminox coverslips (Ted Pella 26028) were sterilized with 70% ethanol and UV irradiation for 1 h prior to coating in the usual fashion (Matrigel for Y6 iPSCs; vitronectin for ACS1028 iPSCs; and fibronectin for iPSC-ECs). Cells were plated and grown as described. At the desired time intervals, the coverslips were removed and placed in warmed (0.1M sodium cacodylate, pH 7.4, 2% paraformaldehyde, and 2.5% glutaraldehyde) and fixed for 60 min at 37°. Cells were then post-fixed in 2% osmium tetraoxide in imidazole buffer 0.1M (pH 7.5) for 1 h, rinsed in distilled water, stained with 3% UA for 1 h, and again rinsed in distilled water. Samples were then dehydrated in ascending grades of acetone, acetone and resin, embedded in a mixture of an Embed 812 kit (EMS 14120), and cured for 48 h in a 60 °C oven.

Ultrathin sections (70 nm) of the organoid were produced using a Leica UltraCut UC6 ultramicrotome, collected on 200 mesh copper grids and post-stained with 3% UA and Reynolds lead citrate. Micrographs were collected using on an FEI Technai Spirit G2 TEM.

Nitric Oxide Synthase Activity Assay

Nitric oxide synthase activity was measured using the DAF-FM kit from Thermo fisher (part number D23842) and read on a Syngene microplate reader in triplicate with an unlabeled control. iPSC-ECs were plated on vitronectin-coated 96-well plates at 25 000 cells/cm^2. After 24 h, cells were labeled with 10 µM DAF-FM and Hoechst 33342 at 5 µg/mL (Invitrogen H1399) in 1× PBS with calcium and magnesium for 30 min in a dark 5% CO_2 humidified incubator, washed with 1× PBS, and allowed to de-esterify intracellular diacetates for an additional 30 min in a dark 5% CO_2 humidified incubator. The signal at 488 nm and 360 nm were quantified in a Syngene plate reader.

Mitophagy and Autophagy Induction

Bafilomycin A1 was purchased from Sigma–Aldrich (#B1793) and reconstituted in DMSO. Antimycin A1 was purchased from Sigma (#A8674) and reconstituted in ethanol. Oligomycin was purchased from Sigma (#75351) and reconstituted in DMSO. FCCP was purchased from Abcam (#ab120081) and reconstituted in DMSO. ULK1 kinase inhibitor SBI-0206965, known to inhibit autophagy, was purchased from Selleck Chemicals (#S7885) and reconstituted in DMSO.[9] Rapamycin was purchased from MP Biomedicals (#159346) and reconstituted in DMSO. Resveratrol was purchased from Sigma (R5010) and reconstituted in DMSO. ML246 and Rg2 were kindly provided by the lab of Dr Congcong He and reconstituted in DMSO.[10,11]

Data Analysis and Statistics

There were 3 biological replicates for each group in each experiment, unless otherwise specified. For MitoTracker quantification, the total fluorescence signal for the area was measured in Fiji and divided by the number of nuclei present. This was done for 5 fields of view (technical replicates) and averaged to generate a data point for a given biological replicate. For the DAF-FM reduction measurements for NO production, a given experimental condition was plated into 3 wells of a 96-well plate. For TEM analysis, each biological sample was imaged in a minimum of 5 locations. Three representative images from each condition were utilized for quantifying autolysosomes per high power field (HPF) in each of 2 separate experiments. For light microscopy images, cells were manually counted from 3 distinct areas of a given experimental condition on 2 separate occasions. All data were analyzed with one-way ANOVA with a post-hoc Tukey test in IBM SPSS Statistics for Macintosh, version 27 (IBM Corp., Armonk, NY, USA). A P value of ≤.05 was considered significant, where * represents comparisons between the specified groups.

Results

iPSCs Successfully Differentiate into Endothelial Cells But Rapidly Lose Key Phenotypic Markers and Proliferative Capacity After a Few Passages

To validate the pluripotency of our iPSC lines, we demonstrated positive immunostaining of lines ACS1028 and Y6 for pluripotency markers by flow cytometry (Supplementary Fig. S1A). Both iPSC lines were differentiated to endothelial cells using the protocol by Patsch et al. occurring over 6 days, passing through lateral mesoderm in the first 3 days.[7] To verify the success of our differentiations, we measured the expression of endothelial cell markers CD144 and CD31 as well as expression of pluripotency markers on each of the 6 days of differentiation by immunostaining and by flow cytometry, with differentiation efficiencies ranging from 20% to 60% CD144+ cells per experiment (Supplementary Fig. S1A, S1B). Pluripotency marker NANOG disappeared by day 5 and pluripotency marker OCT4 began to decrease on day 4 suggesting directed differentiation to endothelial cells in a similar progression to Patsch et al.[7] This order has been suggested as NANOG likely plays a role in modulating Oct4 as a downstream gene.[12] On day 6 the endothelial cells were purified by magnetic associated cell sorting (MACS) for CD144. The resulting endothelial cells demonstrated normal spindle morphology and produced nitric oxide. These results demonstrate the successful loss of pluripotency and acquisition of mature endothelial cell markers and function over the course of the directed differentiation protocol.

To evaluate endothelial cell function over serial passages in culture, we examined typical morphology, as well as CD144 and CD31 expression and proliferation. Immunofluorescence confirmed the loss of morphology as well as CD144 and CD31 expression over serial passages in culture for both Y6-derived ECs and ACS1028-derived ECs (Fig. 1A). At passage 2, CD144 expression was already decreased, 92%-76%, finally nadiring at 30% in passages 4 and 5 (Supplementary Fig. S1C). To evaluate cellular proliferation, we labeled iPSC-ECs with Edu, which is incorporated into replicating DNA and can be fluorescently labeled through click chemistry. iPSC-derived endothelial cell proliferation decreased significantly over serial passages, from 52% staining positive for 5-ethynyl-2′-deoxyuridine (EdU) to 30% from passage 0 to passage 1, nadiring at 10% in subsequent passages (Fig. 1B). The iPSC-derived endothelial cells were unable to be sub-cultured beyond 4 weeks, more commonly only for 3-4 passages over 2 weeks, post cell sorting due to replicative senescence (loss of proliferation by passage 3 shown in Fig. 1B). Our results demonstrate loss of mature endothelial cell markers and proliferative capacity over just a few cultures in the passage.

Autophagy Plays an Active Role During Directed Differentiation of iPSCs to ECs by Recycling Mitochondria Through Mitophagy

Our group and collaborators previously demonstrated that senescence in iPSC-ECs can be attenuated by overexpression of sirtuin1 on a lentivirus.[5] To facilitate future translational applications for iPSC-ECs, we sought to identify small molecules that may enhance the longevity of iPSC-ECs. We investigated autophagy, a known downstream target of sirtuin1 signaling and a mediator of cellular senescence. Autophagy is the process of cellular self-digestion to remove defective intracellular components and recycle them. This process occurs by engulfing the content to be degraded in the autophagosome, which then fuses with a lysosome to form an autolysosome, leading to the degradation of the enclosed contents. A key step in the formation of the autophagosome is the conversion of the cytosolic form of microtubule-associated proteins 1A/1B light chain 3B (LC3-I)

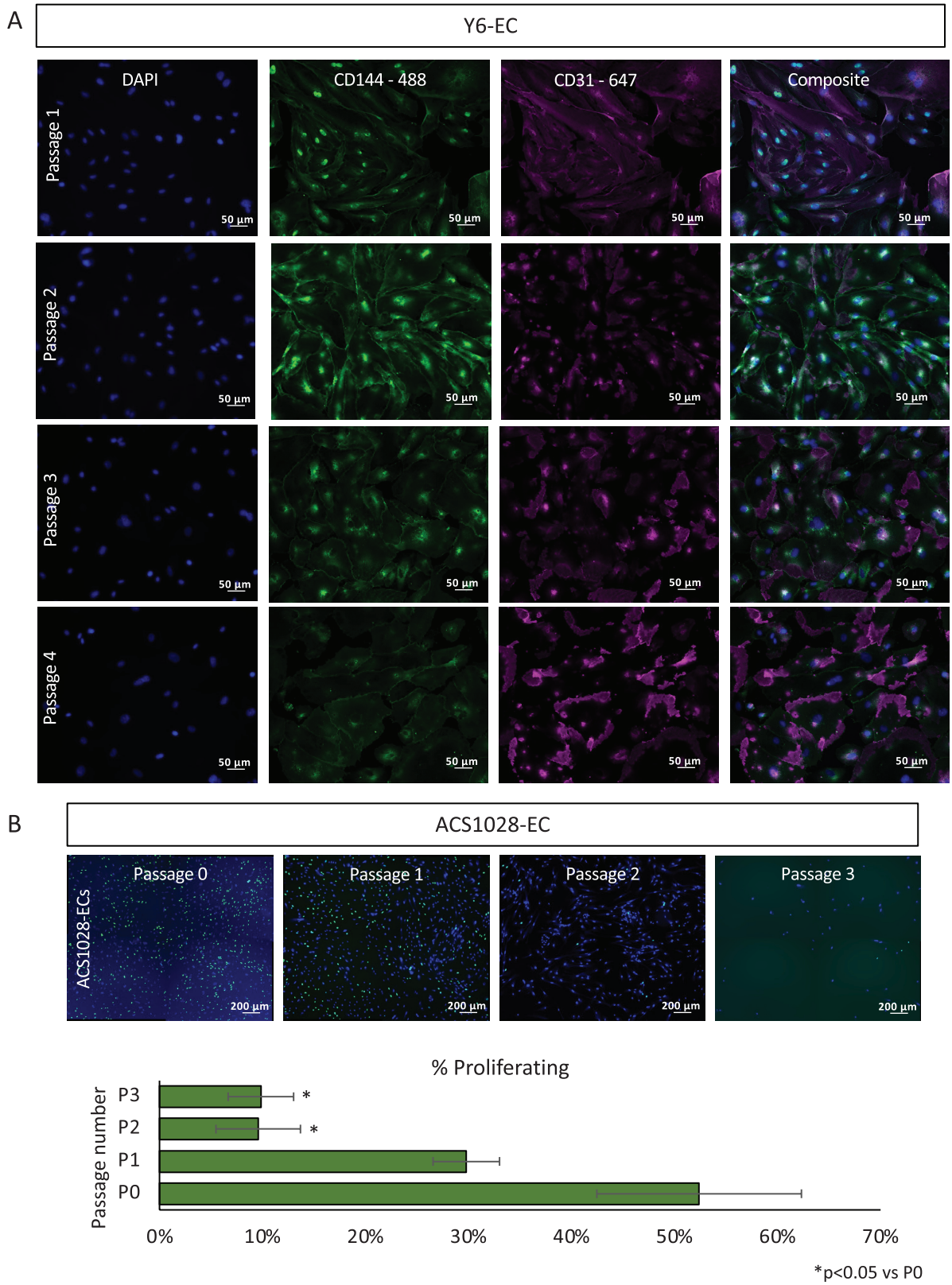

Figure 1. Loss of CD144 and CD31 expression over serial passages correlated with a loss of cellular proliferation. (**A**) Immunofluorescence confirmed the loss of CD144 and CD31, as well typical morphology, over serial passages of purified iPSC-ECs. (**B**) iPSC-ECs demonstrated a decrease in the percent of cells proliferating by EdU labeling over serial passages in culture.

to the lipidated autophagosome-associated form LC3-II by post-translational modification. The drug bafilomycin A1 is utilized to optimize the detection of autophagy induction as it prevents the fusion of the autophagosome to the lysosome, thereby blocking the degradation of newly formed LC3-II and other autophagosome contents by lysosomes.

To understand the role autophagy plays in directed differentiation, LC3-II levels were quantified in iPSCs each of the 6 days during differentiation to ECs by Western blotting whole cell lysates in the presence or absence of 100 nM bafilomycin A1 for 3 h. Optimal bafilomycin treatment was determined empirically for each iPSC line utilized. LC3-II expression normalized to GAPDH was used for quantitation, as it is a more reliable marker of autophagosome formation. LC3-I expression was noted to be lower than LC3-II and was sometimes not visible in the linear range for LC3-II. This may not be indicative of a lost signal, but rather a lower signal in general, as the LC3-I signal is not optimally sensitive in blotting.[8] Therefore, the LC3-II signal, normalized to GAPDH, was measured each day of differentiation. The difference between LC3-II levels without bafilomycin A1 relative to total LC3-II levels reflects autophagosome turnover (flux), whereas high total LC3-II levels represent high autophagosome formation (induction). The two iPSC lines varied slightly in the pattern of autophagy flux and autophagy induction over the course of differentiation. Overall, both lines experienced small, though not statistically significant fluctuations in LC3-II formation (Fig. 2A, S2A). However, by TEM imaging in bafilomycin A1 treated Y6 cells, autolysosomes significantly increased in number from day 2 to day 3 by 19-fold ($P < .05$) and remained abundant through day 6 (Fig. 2B). These data suggest dynamic autophagy activity during differentiation of Y6 iPSCs to ECs. In the ACS1028 line, autolysosomes similarly increased >9-fold in number on day 2 ($P < .05$) and remained numerous through day 6 (Supplementary Fig. S2B). The fluctuations in LC3-II levels and autolysosome numbers in multiple iPSC lines suggest that autophagy is highly dynamic and plays a crucial role during the directed differentiation of iPSCs to ECs.

Mitophagy, the process by which autophagy engulfs and turns over mitochondria,[13] contributes to cell fate reassignment in the process of generating iPSCs from terminally differentiated cells.[14] To assess the role mitophagy plays here in the opposite process of differentiating iPSCs to ECs, we quantified the number of autolysosomes containing mitochondria, indicative of active mitophagy, on each of the different days of differentiation. By TEM, multiple mitochondria were visualized within autolysosomes on days 3-6, but none on days 1 and 2 in both iPSC lines (Fig. 2B, 2C and Supplementary Fig. S2B, S2C). Furthermore, mitochondrial morphology started round, immature and small on day 1, but by day 6 the mitochondria were long and filamentous with obvious cristae (representative image in Fig. 2D). Together these data demonstrate that mitophagy contributes to major changes in mitochondrial remodeling during differentiation, particularly during the late mesoderm phase and the committed phase from days 3 to 6.

iPSC-ECs Demonstrate Decreased Mitophagy Over Serial Passages in Culture

To further evaluate the effects of mitophagy on the mitochondria, we looked for changes in mitochondrial morphology and quantity by performing mitochondrial staining on each day of differentiation. MitoTracker signal was measured by live cell fluorescence microscopy to quantity mitochondrial mass on each day of differentiation. This enabled us to correlate serial changes in mitochondrial remodeling with autophagy activity. Two stains were utilized, red and green, to independently verify the mitochondrial quantity. Fluorescence signals were quantified and averaged on a per cell basis. Both iPSC lines experienced small not statistically significant fluctuations in MitoTracker staining during the course of differentiation (Fig. 3A and Supplementary Fig. S3A, top and bottom panels each).

To evaluate the role of mitophagy in purified iPSC-ECs over serial passages, mature iPSC-derived ECs were also stained with MitoTracker red and green. For both ACS1028-derived ECs and Y6-derived ECs, there was a significant accumulation of mitochondria with a greater than 20-fold increase over serial passages ($P < .05$) (Fig. 3A and Supplementary Fig. S3A, middle and bottom panels each). Specifically, purified iPSC-ECs (ACS1028) demonstrated a 13- and 28-fold increase in total mitochondrial mass at passages 2 and 3, respectively, compared with day 6 of the directed differentiation. This increase remained stable through passage 5, at which time the cells demonstrated replicative senescence. In the Y6-derived ECs, MitoTracker staining increased greater than 20-fold at passage 1 and remained increased through passages 3 and 4. At this time the cells demonstrated replicative senescence.

Mitophagy is known to play a critical role in stem cell differentiation.[15] To further evaluate whether this accumulation of mitochondria may be a failure of mitophagy, autophagy activity was measured over serial passages. In Y6-derived endothelial cells, the total LC3-II level increased at passage 1 but then decreased and remained steady at levels comparable to the level on day 6 (Fig. 3B). The total LC3-II level plateaued and remained stable compared to the level detected on day 6 in ACS1028-derived endothelial cells (Fig. S3B). Similarly, the total number of autolysosomes remained steady over serial passages in both lines (Fig. 3C, 3D, Supplementary Fig. S3C, S3D). Autolysosomes containing mitochondria were absent at later passages despite a comparable number of total autolysosomes (Fig. 3E, Supplementary Fig. S3E). These findings suggest that autophagy, more specifically, mitophagy, is not recycling mitochondria in later passages.

Hypoxia Reduces but does not Eliminate Mitochondrial Accumulation

Given that oxidative damage leads to mitochondrial dysfunction,[13] we hypothesized that the supraphysiologic oxygen concentration of standard culture conditions was contributing to mitochondrial accumulation and to the premature senescence phenomena. To evaluate the effect of hypoxia on mitochondrial accumulation, we cultured iPSC-ECs under normoxic (21%) and hypoxic (1.5%) conditions. A schematic diagram of the experimental design is illustrated in Fig. 4A. Each passage was stained with MitoTracker, green and red, and imaged (Fig. 4B, S4B top row). Signal intensity per cell was calculated and normalized to MitoTracker green staining from normoxic cells at passage 0 for each cell line. Cells cultured in hypoxic conditions demonstrated decreased mitochondria per cell by MitoTracker green and red staining when compared with cells grown under normoxic conditions at the same passage, which reached statistical significance in later passages(Fig. 4B, Supplementary Fig. S4C). This was true for iPSC-derived ECs from both ACS1028 and Y6 lines. Both lines, however, continued to demonstrate an increase in mitochondria per cell over serial passages, although less so under hypoxic conditions. These results demonstrate that hypoxia decreases but does not eliminate the accumulation of mitochondria over serial passages of iPSC-ECs.

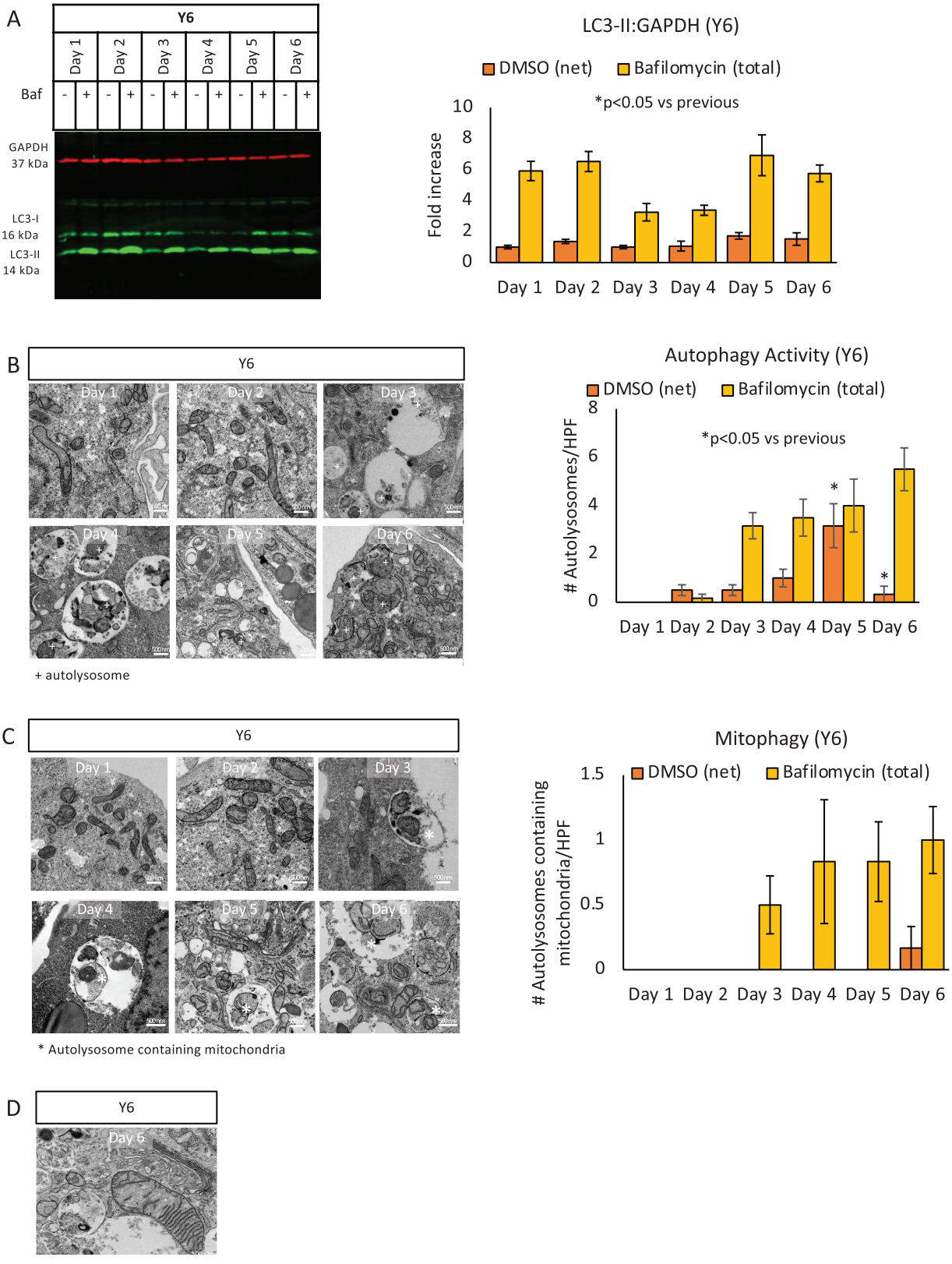

Figure 2. Autophagy plays a critical role and recycles mitochondria during the course of differentiation of Y6 cells. (**A**) In directed differentiation of Y6, total LC3-II decreased from days 2 to 3 and increased from days 4 to 5. (**B**) TEM images of Y6 during differentiation demonstrated a significant increase in number of autolysosomes from days 2 to 3 ($P < .05$), and illustrated the evolving mitochondrial morphology, from immature on day 1 to complex and prototypical on day 6. (**C**) TEM showed autolysosomes recycling mitochondria starting on day 3 of differentiation. (**D**) Representative image of a mature mitochondria on day 6 of differentiation.

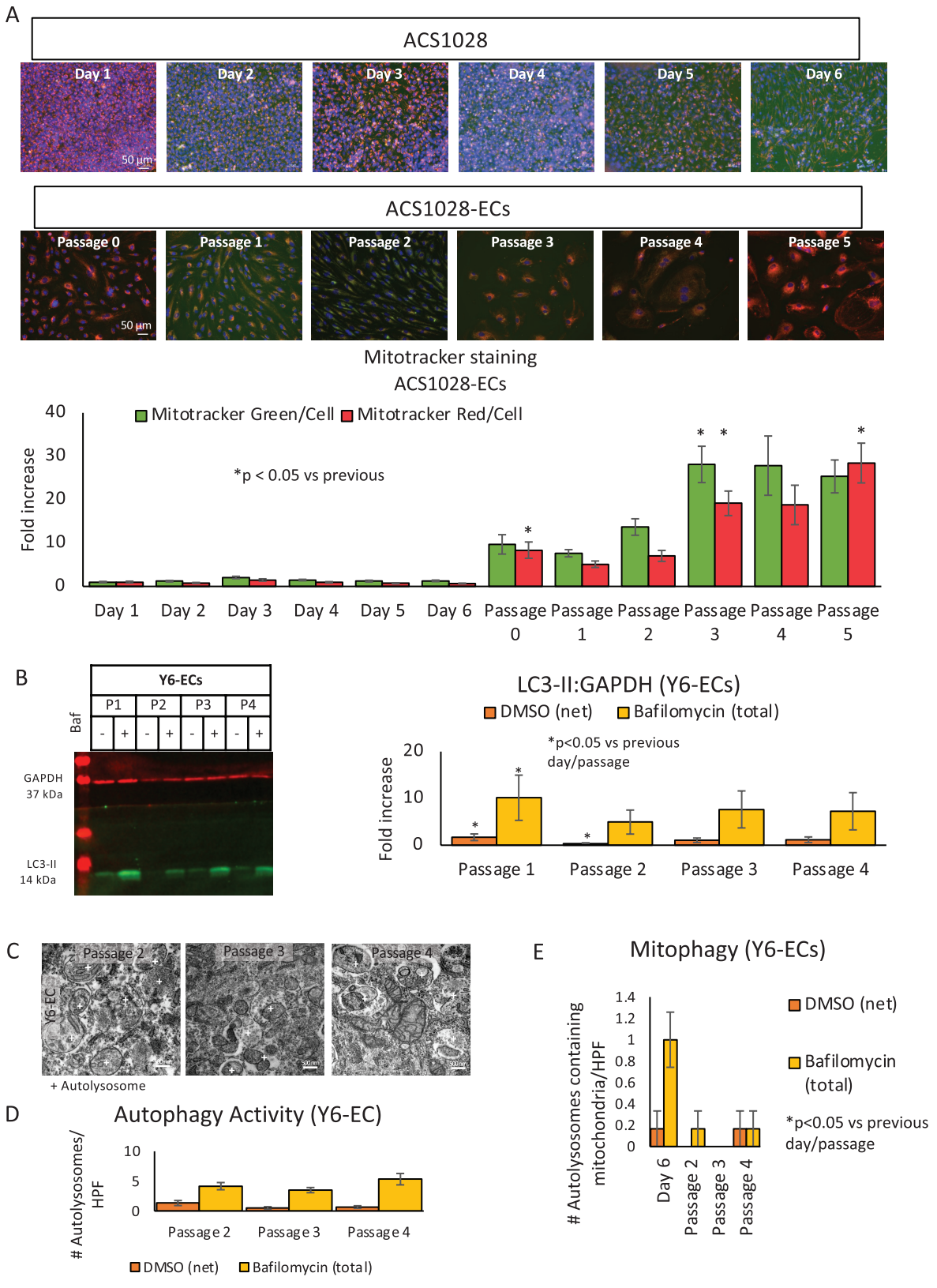

Figure 3. Mitochondria accumulate over serial passages in ACS1028-ECs without a compensatory increase in recycling. (**A**) Top panel: MitoTracker staining of ACS1028 cells on each day of differentiation to ECs demonstrated that mitochondrial mass and morphology change over the course of differentiation. Middle panel: MitoTracker staining of each passage of ACS1028-ECs showed mitochondrial accumulation in later passages. Bottom panel: Quantification of average MitoTracker signal per cell by fluorescence microscopy revealed a significant and greater than 20-fold increase in mitochondria in iPSC-ECs ($P < .05$). (**B**) LC3-II expression remained stable throughout serial passages of Y6-ECs. (**C-D**) Representative TEM images of Y6-ECs from each passage showing a stable number of autolysosomes over serial passages. (**E**) Quantification of autolysosomes containing mitochondrial structures demonstrated a decrease in mitophagy in Y6-ECs compared to during differentiation ($P < .05$).

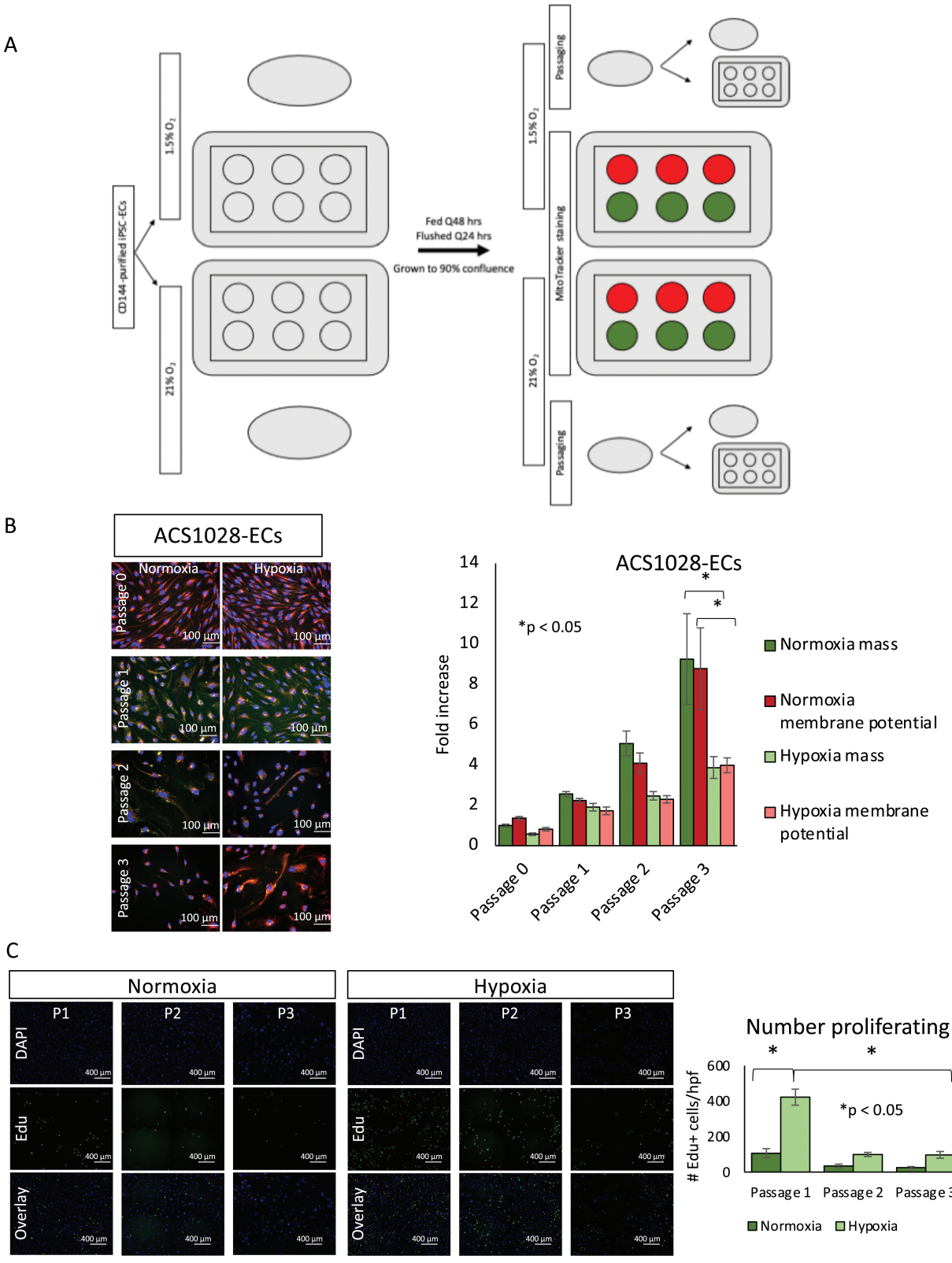

Figure 4. Hypoxia reduced MitoTracker staining per ACS1028-EC cell at each passage but still resulted in loss of proliferation over serial passages. (**A**) Schematic diagram of hypoxia experiment. (**B**) 1.5% oxygen reduced MitoTracker red and green staining per ACS1028-EC cell compared to normoxic conditions at early passages but cells ultimately accumulated mitochondria in later passages. (**C**) ACS1028-EC proliferation was improved under hypoxic conditions but still declined over serial passages.

To assess the effect of hypoxia on proliferation, we labeled cells at each passage with EdU. This demonstrated an increase in the number of proliferating cells at passage 1 under hypoxic conditions as compared with normoxia in ACS1028-ECs, but this was not sustained over serial passages (Fig. 4C). Similarly, for Y6-ECs, we counted nuclei per high power field over 5 areas for each of 3 biological replicates, which demonstrated an increased number of cells under hypoxic conditions compared with normoxic conditions in initial passages that did not sustain over serial passages (Fig. S4D). Cell numbers did still diminish in later passages under both conditions for both cell lines. These results demonstrate that hypoxia improves proliferation and survival, but iPSC-ECs still reach replicative senescence even under hypoxic conditions.

We further evaluated iPSC-EC function under hypoxic conditions by examining morphology and staining for key markers CD144 and CD31, as well as assessing NO production. While we found that surviving cells did express CD144 and CD31 by immunostaining, the cells still demonstrated the same loss of typical morphology with non-uniform membrane staining at later passages under both normoxic and hypoxic conditions, which suggests the cells still lost mature cell properties even under hypoxic conditions (Supplementary Fig. S4A, S4B lower rows). Interestingly, NO synthase activity did not differ in early passages between normoxic and hypoxic conditions but was preserved in later passages with hypoxic compared to normoxic conditions (Fig. S4E). Taken together, these results demonstrate that hypoxic conditions improve but do not eliminate mitochondrial accumulation and loss of cellular proliferation and mature phenotype.

Since hypoxia did not resolve the mitochondrial accumulation, we next evaluated the effect of increasing mitophagy in iPSC-ECs. We cultured ACS1028-ECs in the presence or absence of several different concentrations of known inducers of mitophagy, antimycin A, and oligomycin. The experimental design is presented in Supplementary Fig. S5A. Mitophagy inducers Antimycin A and oligomycin resulted in high levels of cell loss, regardless of concentration (Supplementary Fig. S5B, S5C). This was also true of the mitochondrial uncoupler FCCP, suggesting that iPSC-ECs do not tolerate the loss of mitochondrial membrane potential. We found that surviving cells rapidly lost their CD144 and CD31 uniform membrane staining by passage 1 (Fig. S6A, S6B), which suggests that direct pharmacologic stimulation of mitophagy through membrane depolarization accelerated rather than alleviated the senescence problem.

mTOR-Independent ULK1-Kinase Mediated Autophagy Improves iPSC-EC Proliferation

We next tested whether inducing autophagy in iPSC-ECs would overcome the premature senescence phenomenon. Both autophagy inducer resveratrol and autophagy inhibitor SBI-0206965 impeded cell survival, with no cells surviving to passage 1. Autophagy inducer ML246[10] yielded no viable cells after 24 h at the higher concentrations of 0.5 μM and 0.25 μM. A reduced concentration of 0.125 μM still yielded too few cells for passage (Supplementary Fig. S7A, S7B). Rapamycin, at all tested concentrations, also yielded an insufficient number of cells for passaging (Supplementary Fig. 5A, 5B). Rg2, an mTOR-independent inducer of autophagy,[11] improved cell survival with an increased rate of proliferation (Figure 5A-5C). Due to the loss of proliferating cells in the control culture, the experiment was terminated at passage 3. The effect of Rg2 persisted through passage 3, although the number of total and proliferating cells were fewer after 4 days in the culture at passage 3 than at passage 0 (Fig. 5C). As Rg2 is known to be mTOR-independent, and rapamycin did not produce any beneficial results to proliferation, these results suggest that Rg2 produces a beneficial effect on iPSC-EC longevity through an mTOR-independent pathway.

To assess whether the effect of Rg2 on proliferation is mediated through autophagy, we co-treated ACS1028-ECs with 200 μM Rg2 and SBI-0206965 to block ULK1 kinase at varying concentrations. We assessed cell survival by counting the number of cells per high power field by light microscopy, which diminished over serial passages in the DMSO-treated vehicle-control condition, as expected. Decreased cell survival to passage 3 demonstrated a dose-dependent response to SBI-0206965 in the presence of 200 μM Rg2, with fewer cells surviving when treated with higher concentrations of SBI-0206965 (Fig. 6A, Supplementary Fig. S7C). At the highest concentration of SBI-020965 used, 10 μM, there were almost no surviving cells in passages 2 and 3. We found that at passage 3, the Rg2 treated cells demonstrated an increase in LC3-II level by Western blotting, which was reduced by the addition of ULK1 kinase inhibitor SBI-0206965 at any concentration (Fig. 6B, 6C), suggesting that the longevity-enhancing increased LC3-II level was mediated by ULK1 kinase autophagy.

Discussion

Autophagy plays a significant role in the differentiation and culture of iPSC-ECs. This was seen in our study as significant changes in autolysosome numbers over the different days of differentiation. This correlated with changes in the maturity of mitochondria, with direct evidence of mitophagy occurring in the mid to later stages of differentiation. In the culture of purified iPSC-ECs, mitochondria have increased MitoTracker staining per cell, suggestive of mitochondrial accumulation. However, this reached a plateau after several passages and was accompanied by replicative senescence. It is possible that the iPSC-ECs are experiencing endothelial-to-mesenchymal transition globally; regardless, this loss of function presents a barrier to translational applications. Hypoxia conferred a transient benefit to the proliferation rate, but autophagy inducer Rg2 produced the most potent benefit, an improvement that was dependent on ULK1 signaling and was independent of mTOR.

While autophagy plays a crucial role in the differentiation process, we focused our study on the manipulation of autophagy in the post-differentiation culture stage for iPSC-ECs. Autophagy has previously been demonstrated to be critical to stem cell function, and interruption of autophagy results in significant stem cell dysfunction and death.[14,16,17] Gross modulation of autophagy during differentiation is likely to produce large-scale effects and is unlikely to be compatible with successful and controlled directed differentiation to the target cell type. Furthermore, the regulation of differentiation involves a highly complex interaction of a multitude of signals. Computational systems biology approaches to further optimize specifically directed differentiation protocols hold great promise for enhancing this highly complex biologic process.[18-21]

In our study, hypoxia conferred an initial benefit. It is possible that mitochondrial oxidative damage could be

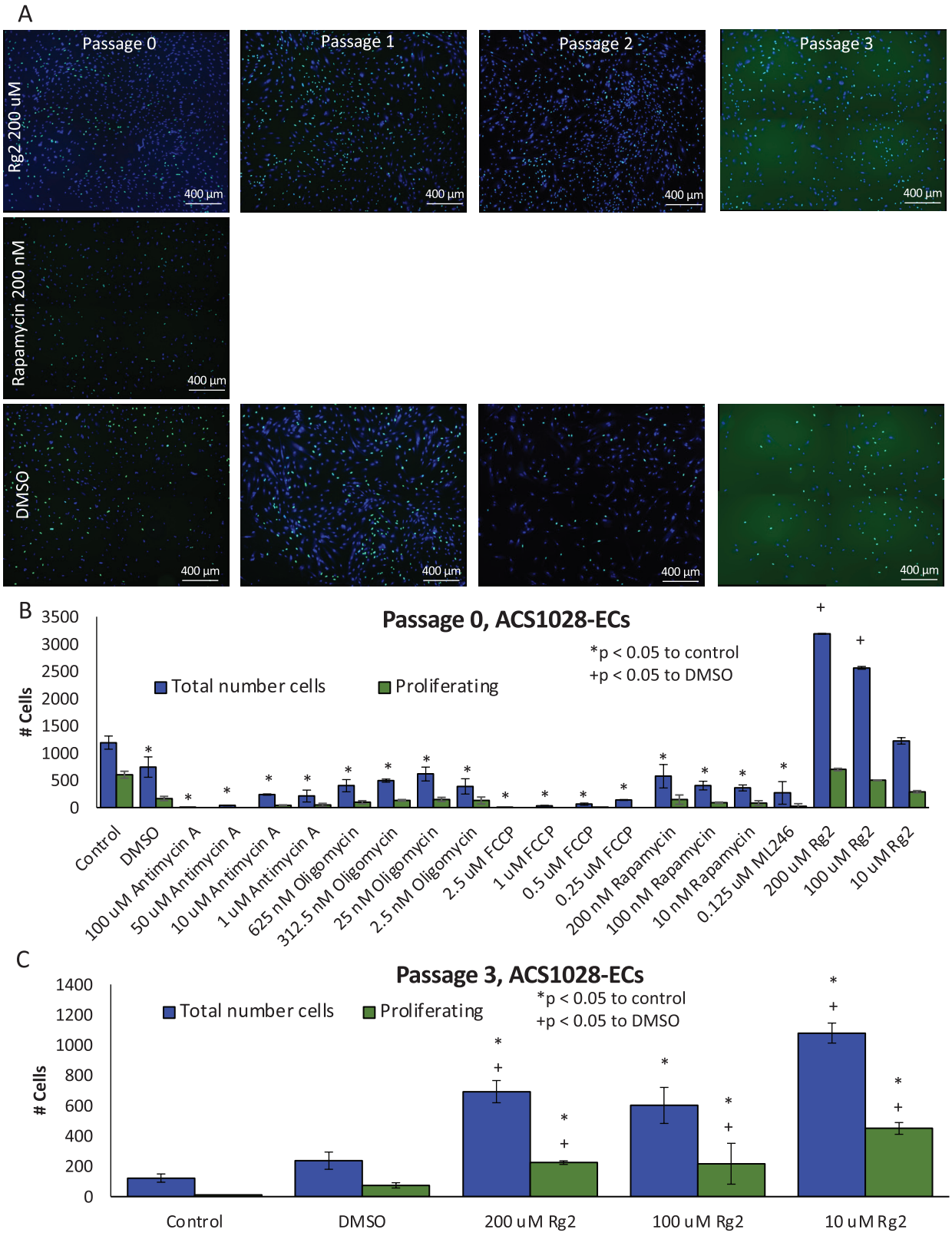

Figure 5. Plant derivative Rg2 improved proliferation of ACS1028-ECs over serial passages. (**A**) EdU labeling of ACS1028-ECs treated with Rg2, rapamycin or DMSO as a vehicle control demonstrated improved proliferation with Rg2 treatment. (**B**) Quantification of EdU labeled cells demonstrated a statistically significant improvement in proliferation with Rg2 treatment compared to treatment with rapamycin, ML246, or mitophagy inducers Antimycin A or oligomycin. (**C**) The benefit to proliferation conferred by Rg2 was sustained through passage 3.

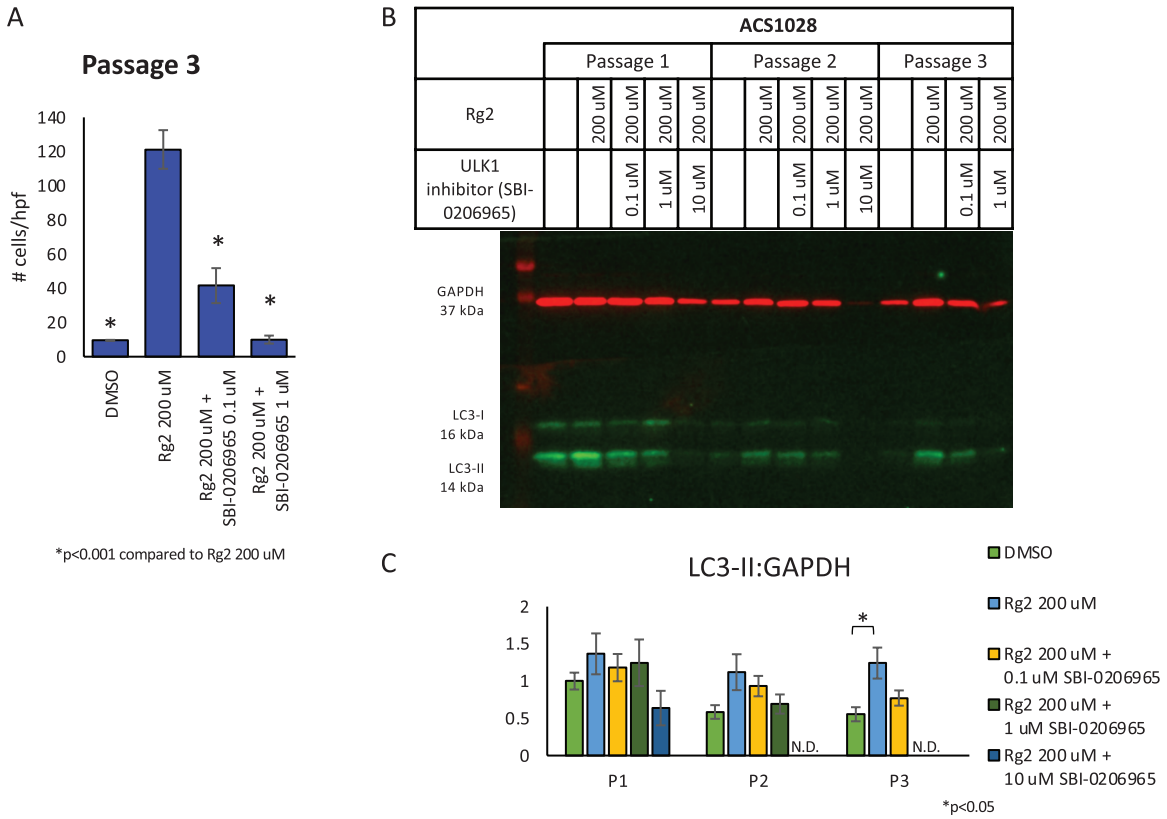

Figure 6. Ulk1 kinase inhibitor SBI-0206965 blocked the survival benefit associated with increased LC3-II that was conferred by Rg2. (**A**) Manual counting of cells in light microscopy demonstrated a statistically significant reduction in cell survival in a dose-dependent manner when cells were co-treated with SBI-0206965 in the presence of Rg2. (**B-C**) Western blotting of ACS1028-EC lysate from serial passages treated with DMSO as a control, or with Rg2, or with Rg2 and various concentrations of SBI-0206965 demonstrated a significant increase in LC3-II expression with Rg2 treatment at passage 3 that is attenuated by co-treatment with SBI-0206965.

contributing to the proliferative senescence witnessed in iPSC-ECs; however, the cellular proliferation rate did slow over serial passages. Pluripotent stem cell (PSC) derived cardiomyocytes, from either embryonic stem cells or iPSCs, similarly demonstrate significant changes in mitochondrial abundance and maturity over time in culture that differs from fetal cardiomyocyte tissue. Between days 50 and 100, fetal cardiomyocytes experience significant increases in respiratory chain complex activity; in this time frame, however, PSC-derived cardiomyocytes do not significantly enhance the activity of their respiratory chain complexes.[22] Human cardiac progenitor cells—adult stem cells—from heart failure patients also display early senescence mediated by oxidative damage under standard culture conditions. This is mitigated by growth in hypoxic culture conditions with 1% O_2, associated with improved mitochondrial function, decreased mitochondrial abundance, and decreased senescence. This benefit from hypoxia was reversed by the addition of Antimycin A to induce oxidative stress.[23] There will likely be a degree of difference between endothelial cells and cardiomyocytes, and between PSCs and adult stem cells, in the signals required to preserve longevity under culture conditions. Overall, given the short-lived benefit of hypoxia for the iPSC-ECs seen here, these results suggest that the accumulation of MitoTracker staining in later passages is not simply the result of oxidative damage from supraphysiologic oxygen levels in culture conditions but a more complex multifactorial process involving mitochondrial quality control. Mitophagy has been identified as a key regulator of stem cell function, and our findings suggest it continues to play a role in the identification and quality of cells differentiated from iPSCs.[24] Further studies manipulating the genetic regulators of mitophagy, such as Parkin and PINK1, will be imperative to further elucidate this mechanism.[25]

Rg2 demonstrated the most potent effect on iPSC-EC proliferation in culture. The effect of Rg2 correlated with LC3-II levels and was mitigated by SBI-0206965, demonstrating that it is mediated through ULK1 kinase autophagy. However, this benefit was not reproduced with rapamycin treatment, suggesting that Rg2 is conferring this benefit through mTOR-independent autophagy. Rg2 was previously demonstrated to act through AMP kinase activation, which may also explain our observations here.[11] Interruption of the ULK1-AMP kinase pathway has been demonstrated to disrupt mitophagy, which could explain some of the beneficial effects seen with our iPSC-ECs.[15] In addition, lentiviral mediated SIRT1 overexpression in iPSC-ECs enhanced longevity, as did nutrient starvation.[5,6] The ULK1-AMP kinase pathway was also implicated in the stabilization of SIRT1 by nitric oxide in HUVECs.[26] This, along with our data here, suggest that endothelial cells promote longevity by stabilizing SIRT1 expression through nitric oxide-mediated ULK1-dependent autophagy. The specific mechanisms of the beneficial effect of Rg2 for iPSC-ECs may be multi-factorial. It will be important in future studies to corroborate the effect of autophagy enhancement

through genetic repression and stimulation of autophagy in iPSC-ECs, which will also further refine the specific pathways responsible for this effect.

While our results demonstrate a significant improvement in iPSC-EC proliferation and viability with ULK1-mediated autophagy when treated with Rg2, there are some limitations to this study. Different iPSC lines have been shown to exhibit discrepant behaviors when exposed to a given stimulus; likely the future of translational applications will depend in part on identifying specific clones from a given patient sample that will achieve the desired result. Furthermore, some methods for quantifying autophagy activity have their own limitations. LC3-II levels can be influenced by processes aside from autophagy activity. However, in the present study, we demonstrated reproducible and significant biologic outcomes in separate iPSC lines, and we further interrogated autophagy with TEM imaging of autolysosomes in each of these distinct lines.

Summary

This work highlights the importance of autophagy in the differentiation and phenotypic longevity of iPSC-ECs. Our findings specifically show that premature senescence can be attenuated with small molecule treatment to augment mTOR-independent ULK1-mediated autophagy, a method that, unlike viral transduction, is readily translated to clinical use. This biologic effect of autophagy identified here opens the door to identifying new targets to improve iPSC-ECs and overcomes a major barrier to utilizing patient-derived stem cells for clinical applications.

Acknowledgements

The authors would like to thank Karen Ho, M.D., for her conceptual contributions to this project at various stages. The iPSC line Y6 was generated by the Yale Stem Cell Center. Authors K.E.H., K.K. and J.A.W. were affiliated with Northwestern University during the time this project was completed; K.E.H. is now affiliated with Emory University, and the Atlanta VA Healthcare System and K.K. and J.A.W. are currently affiliated with the University of Arizona and the Southern Arizona VA Healthcare System. The content is solely the responsibility of the authors and do not represent the views of the National Institutes of Health.

Funding

This work was supported by NIH F32HL137292, the Robert R. McCormick Foundation, the Bright Focus Foundation via the Alzheimer's Disease Research Award, NIH R01DK113168, NIH R01DK113170 and NIH R01DK123447. This research was supported in part by the Ruth L. Kirschstein National Research Service Award from the National Heart, Lung, and Blood Institute of the National Institutes of Health under award number F32HL137292 (K.E.H), and grants from the Robert R. McCormick Foundation (J.A.W.) and from BrightFocus Foundation via the Alzheimer's Disease Research Award (C.H.), as well as by the National Institute of Diabetes and Digestive and Kidney Disease of the National Institutes of Health under award numbers R01DK113168 (J.A.W.), R01DK113170 (C.H.) and R01DK123447 (C.H.). This work made use of the (Re) Building a Kidney Coordinating Center funded by the National Institute of Diabetes and Digestive and Kidney Diseases of the National Institutes of Health under award number U01DK107350. This work was supported by the Northwestern University RHLCCC Flow Cytometry Facility and a Cancer Center Support Grant (NCI CA060553) and by the Northwestern University Pathology Core Facility and a Cancer Center Support Grant (NCI CA060553). Imaging work was performed at the Northwestern University Center for Advanced Microscopy generously supported by NCI CCSG P30CA060553 awarded to the Robert H. Lurie Comprehensive Cancer Center.

Conflicts of Interest

The authors declared no potential conflicts of interest.

Author Contributions

K.H.: conception and design, financial support, collection and assembly of data, data analysis and interpretation, manuscript writing, final approval of manuscript. K.K.: conception and design, collection and assembly of data, manuscript writing, final approval of manuscript. D.I.: conception and design, collection and assembly of data, manuscript writing, final approval of manuscript C.H.: conception and design, provision of study material, data analysis and interpretation, final approval of manuscript. J.W.: conception and design, financial support, administrative support, provision of study material, data analysis and interpretation, final approval of manuscript.

Data Availability

The data that support the findings of this study are available from the corresponding author upon reasonable request.

Supplementary Material

Supplementary material is available at *Stem Cells Translational Medicine* online.

References

1. Banito A, Gil J. Induced pluripotent stem cells and senescence: learning the biology to improve the technology. *EMBO Rep.* 2010;11(5):353-359. https://doi.org/10.1038/embor.2010.47
2. Menendez JA, Vellon L, Oliveras-Ferraros C, et al. mTOR-regulated senescence and autophagy during reprogramming of somatic cells to pluripotency: a roadmap from energy metabolism to stem cell renewal and aging. *Cell Cycle.* 2011;10(21):3658-3677. https://doi.org/10.4161/cc.10.21.18128
3. Li Z, Hu S, Ghosh Z, et al. Functional characterization and expression profiling of human induced pluripotent stem cell- and embryonic stem cell-derived endothelial cells. *Stem Cells Dev.* 2011;20(10):1701-1710. https://doi.org/10.1089/scd.2010.0426
4. Wimmer RA, Leopoldi A, Aichinger M, et al. Human blood vessel organoids as a model of diabetic vasculopathy. *Nature.* 2019;565(7740):505-510. https://doi.org/10.1038/s41586-018-0858-8
5. Jiang B, Jen M, Perrin L, et al. SIRT1 overexpression maintains cell phenotype and function of endothelial cells derived from induced pluripotent stem cells. *Stem Cells Dev.* 2015;24(23):2740-2745. https://doi.org/10.1089/scd.2015.0191
6. Gokoh M, Nishio M, Nakamura N, et al. Early senescence is not an inevitable fate of human-induced pluripotent stem-derived cells.

Cell Reprogram. 2011;13(4):361-370. https://doi.org/10.1089/cell.2011.0004
7. Patsch C, Challet-Meylan L, Thoma EC, et al. Generation of vascular endothelial and smooth muscle cells from human pluripotent stem cells. *Nat Cell Biol*. 2015;17(8):994-1003. https://doi.org/10.1038/ncb3205
8. Mizushima N, Yoshimori T. How to interpret LC3 immunoblotting. *Autophagy*. 2007;3(6):542-545. https://doi.org/10.4161/auto.4600
9. Egan DF, Chun MG, Vamos M, et al. Small molecule inhibition of the autophagy kinase ULK1 and identification of ULK1 substrates. *Mol Cell*. 2015;59(2):285-297. https://doi.org/10.1016/j.molcel.2015.05.031
10. Rocchi A, Yamamoto S, Ting T, et al. A Becn1 mutation mediates hyperactive autophagic sequestration of amyloid oligomers and improved cognition in Alzheimer's disease. *PLoS Genet*. 2017;13(8):e1006962. https://doi.org/10.1371/journal.pgen.1006962
11. Fan Y, Wang N, Rocchi A, et al. Identification of natural products with neuronal and metabolic benefits through autophagy induction. *Autophagy*. 2017;13(1):41-56. https://doi.org/10.1080/15548627.2016.1240855
12. Loh Y-H, Wu Q, Chew J-L, et al. The Oct4 and Nanog transcription network regulates pluripotency in mouse embryonic stem cells. *Nat Genet*. 2006;38(4):431-440. https://doi.org/10.1038/ng1760
13. Lee J, Giordano S, Zhang J. Autophagy, mitochondria and oxidative stress: cross-talk and redox signalling. *Biochem J*. 2012;441(2):523-540. https://doi.org/10.1042/BJ20111451
14. Ma T, Li J, Xu Y, et al. Atg5-independent autophagy regulates mitochondrial clearance and is essential for iPSC reprogramming. *Nat Cell Biol*. 2015;17(11):1379-1387. https://doi.org/10.1038/ncb3256
15. Sotthibundhu A, Promjuntuek W, Liu M, et al. Roles of autophagy in controlling stem cell identity: a perspective of self-renewal and differentiation. *Cell Tissue Res*. 2018. https://doi.org/10.1007/s00441-018-2829-7
16. Zhou J, Su P, Wang L, et al. mTOR supports long-term self-renewal and suppresses mesoderm and endoderm activities of human embryonic stem cells. *Proc Natl Acad Sci USA*. 2009;106(19):7840-7845. https://doi.org/10.1073/pnas.0901854106
17. Sotthibundhu A, McDonagh K, von Kriegsheim A, et al. Rapamycin regulates autophagy and cell adhesion in induced pluripotent stem cells. *Stem Cell Res Ther*. 2016;7(1):166. https://doi.org/10.1186/s13287-016-0425-x
18. Zhou J, Sears RL. Bioinformatics approaches to stem cell research. *Curr Pharmacol Rep*. 2018;4(4):314-325. https://doi.org/10.1007/s40495-018-0143-4
19. Bukys MA, Mihas A, Finney K, et al. High-dimensional design-of-experiments extracts small-molecule-only induction conditions for dorsal pancreatic endoderm from pluripotency. *iScience*. 2020;23(8):101346. https://doi.org/10.1016/j.isci.2020.101346
20. Kitano H. Computational systems biology. *Nature*. 2002;420:206-210.
21. Carinhas N, Oliveira R, Alves PM, et al. Systems biotechnology of animal cells: the road to prediction. *Trends Biotechnol*. 2012;30(7):377-385. https://doi.org/10.1016/j.tibtech.2012.03.004
22. Dai DF, Danoviz ME, Wiczer B, et al. Mitochondrial maturation in human pluripotent stem cell derived cardiomyocytes. *Stem Cells Int*. 2017;2017:10. https://doi.org/10.1155/2017/5153625
23. Korski KI, Kubli DA, Wang BJ, et al. Hypoxia prevents mitochondrial dysfunction and senescence in human c-Kit(+) cardiac progenitor cells. *Stem Cells*. 2019;37(4):555-567. https://doi.org/10.1002/stem.2970
24. Guan JL, Simon AK, Prescott M, et al. Autophagy in stem cells. *Autophagy*. 2013;9(6):830-849. https://www.pnas.org/doi/full/10.1073/pnas.0901854106
25. Jin SM, Youle RJ. PINK1- and parkin-mediated mitophagy at a glance. *J Cell Sci*. 2012;125(Pt 4):795-799. https://doi.org/10.1242/jcs.093849
26. Xing J, Liu H, Yang H, et al. Upregulation of Unc-51-like kinase 1 by nitric oxide stabilizes SIRT1, independent of autophagy. *PLoS One*. 2014;9(12):e116165e116165. https://doi.org/10.1371/journal.pone.0116165